The burning mechanism of non-reacted pockets in cellular detonations

Farzane Zangene, Matei I. Radulescu
University of Ottawa
Otatwa, Ontario, Canada

1 Introduction

Detonation waves in gases are characterized by a cellular structure, which controls the overall rate of energy release. Detonation fronts consist of triple shock reflections, which generate a complex pattern of burning gas that, in turn, influences the shock propagation [1]. Experiments have shown the reflection of the waves in the cellular structure, often give rise to shocked unburned pockets of reactive fuel in its wake, which peel away from the main front after triple-point reflections [2–5]. These dense, unburned gas pockets, are a common feature of all detonation cellular structures, particularly in irregular-structure mixtures such as methane–oxygen. Figure 1 presents examples of detonation cellular structures in mixture of $CH_4/2O_2$ at various initial pressures, with arrows highlighting some of the unreacted pockets in the images [6]. The dense unburned gas pockets detach from the main front and are consumed within the timescale of the first triple-point reflection. Understanding the role these unreacted pockets play in sustaining detonation propagation—particularly in mixtures with highly sensitive kinetics and irregular cellular dynamics—is challenging due to the difficulty of experimentally isolating a detonation cell in a reproducible manner.

The objective of this study is to establish the burning mechanism and regression rate of non-reactive pockets in detonation. Building on our previous experimental study [7], where we developed a technique to isolate the triple shock collision process, we now refine this approach to investigate post-reflection dynamics in greater detail. In our earlier work, a detonation wave was transmitted through a bifurcated converging–diverging nozzle, generating a reproducible shock reflection at its exit. At this stage, two transmitted incident shocks interacted to form a new Mach shock. Our observations revealed that, due to the cellular irregularity and the highly sensitive chemistry of the methane–oxygen mixture, the reaction front exhibited significant hydrodynamic fluctuations and persistent unreacted pockets, even in the expanding sections of the channel. These small-scale phenomena likely played a crucial role in the re-ignition process following the reflection. In the new setup, as the detonation wave exits the converging–diverging nozzle, it undergoes laminarization, forming a curved shock-reaction zone structure. Upon frontal reflection at the nozzle exit, a first-generation Mach reflection occurs, triggering exothermicity and generating the desired triple shock structure. With the well-defined laminar detonation at the nozzle exit, our goal is to investigate the burning mechanism of gas pockets and their subsequent feedback into the shock. By generating a reproducible Mach reflection, we can examine this process

Correspondence to: fzang055@uottawa.ca

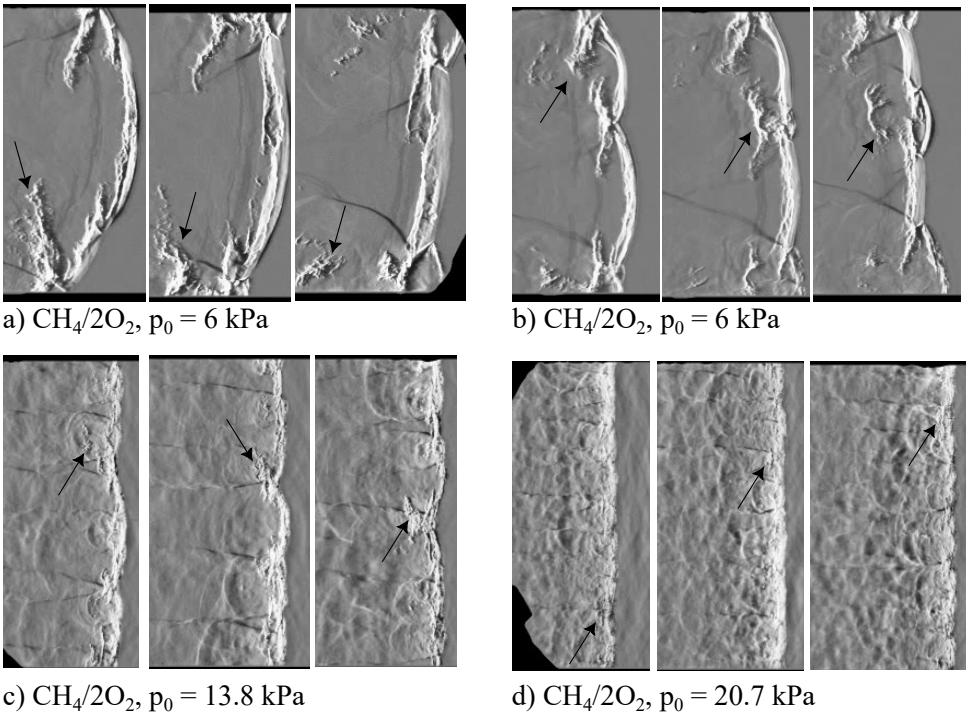

a) $CH_4/2O_2$, p_0 = 6 kPa b) $CH_4/2O_2$, p_0 = 6 kPa

c) $CH_4/2O_2$, p_0 = 13.8 kPa d) $CH_4/2O_2$, p_0 = 20.7 kPa

Figure 1: Schlieren visualization of detonation structures for $CH_4/2O_2$ at various initial pressures.

in detail, using a combination of high-speed videos and pressure transducers. This permits us to reconstruct the internal state of the gas pockets and determine their burning rate. Furthermore, a more accurate reconstruction of the gas state will be achieved through numerical simulations and will be presented in the conference.

2 Experiments

2.1 Experimental details

The experiments were carried out in a rectangular shock tube measuring $3.4\,\mathrm{m}$ in length, $0.203\,\mathrm{m}$ in height, and $0.019\,\mathrm{m}$ in width. The channel, composed of initiation, propagation, and test sections, was constructed from aluminum. A schematic of the experimental setup is shown in Fig. 2, with further details available in previous work [8]. To create a converging–diverging nozzle, two aluminum triangular objects were placed in the test section. The test section featured glass walls to enable visualization of the detonation evolution. A $1\,\mathrm{m}$-long large-scale shadowgraph system was used to capture the detonation process along the entire test section. This system included a $2\,\mathrm{m} \times 2\,\mathrm{m}$ retro-reflective screen and a $1000\,\mathrm{W}$ Xenon arc lamp. High-speed imaging was performed using a Phantom v1210 camera, which operated at $44\,000\,\mathrm{s}^{-1}$, with a resolution of 1024 $\times$ 272 px^2 and an exposure time of $0.47\,\mu\mathrm{s}$. Additionally, a Z-type schlieren system was employed consist of a slit, a vertical knife-edge, a $1000\,\mathrm{W}$ Xenon arc lamp, and two concave mirrors to visualize the details of the triple points reflection. Recordings were made at various frame rates, reaching up to $800\,000\,\mathrm{s}^{-1}$, with a resolution of 400 $\times$ 250 px^2 and an exposure time of $0.2\,\mu\mathrm{s}$, using a Shimadzu HPV-X2 camera.

Seven high-frequency piezoelectric PCB pressure sensors (models 113B24 and 113B27) were mounted on the top wall of the shock tube to record pressure signals and determine the pressure evolution in the post shock region. These sensors have a resonance frequency of $500\,\mathrm{kHz}$, and pressure signals were

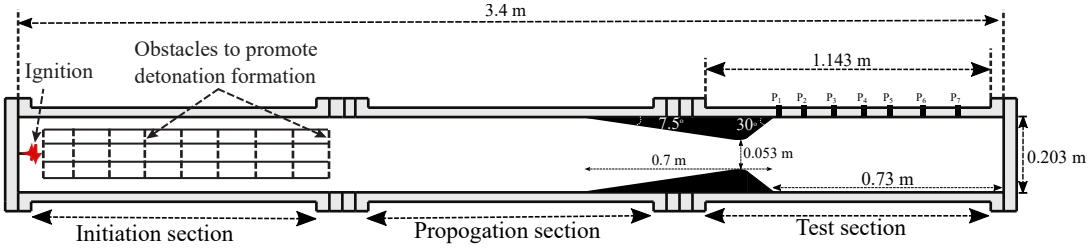

Figure 2: Schematic of the shock tube used in the experiment.

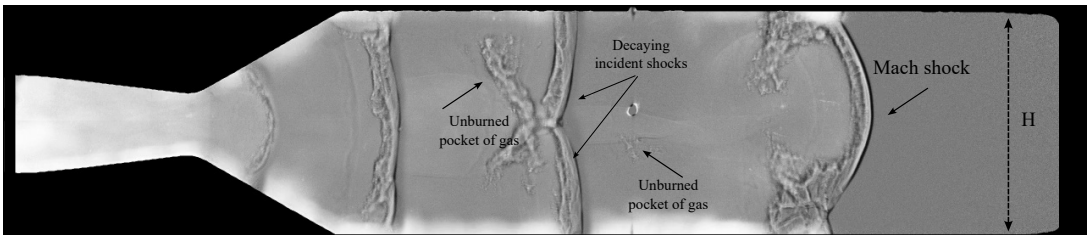

Figure 3: Detonation propagation from left to right in a $CH_4/2O_2$ mixture at $p_0 = 17.2$ kPa and $T_0 = 295$ K. The visualization length is 1000 mm, captured using the shadowgraph technique, with a channel height H of 203 mm.

recorded at a sampling rate of $1.5\,\mathrm{MHz}$ during the experiments. All pressure gauges used had a diameter of $5.5\,\mathrm{mm}$ and a maximum error of 1.3%, as determined from calibration data.

The test mixture was a stoichiometric methane–oxygen mixture ($CH_4/2O_2$), prepared in a separate mixing tank using the method of partial pressures. The gases were allowed to mix for over 24 hours to ensure homogeneity. Prior to filling the shock tube with the test gases, it was evacuated to a pressure below $80\,\mathrm{Pa}$. The premixed combustible mixture was ignited using a custom-designed point igniter consisting of a tungsten wire and a $12\,\mathrm{V}$ battery. Each experiment was conducted five times at each initial pressure to assess reproducibility and determine the standard deviation of the measurements.

2.2 Experimental results

Figure 3 presents the results of the shadowgraph method for a stoichiometric $CH_4/2O_2$ mixture at $p_0 = 17.2$ kPa. The superimposed shadowgraph images illustrate the evolution of the detonation front along the full 1-meter test section. As the detonation wave enters the converging section, it initially becomes overdriven before undergoing laminarization in the diverging section. Upon entering the narrow channel, two Mach shocks form due to reflections from the top and bottom walls, while the central incident shock continues to decay. The accumulation of shocked, unburned gas behind the incident shock is a clear indicator of this decay process. Following the reflection of the two shocks at the center of the test section, an unburned gas tongue separates from the main front and lags behind. Repeated experiments show that these unreacted gas pockets fully burn out within approximately half a detonation cell length—the time corresponding to the next reflection of triple points from the walls, estimated at about 200 microseconds—consistent with the timescale of the detonation cell, as previously observed in Fig. 1. To further visualize the small-scale features, schlieren videos of the same experimental conditions are presented in Fig. 4. The schlieren images capture a sequence of frames showing the detonation wave propagating over a 30 cm distance (matching the mirror diameter). The detonation propagates from left to right, revealing key features such as long-tailed transverse shocks, fine-scale dense unreacted gas pockets breaking away from the irregular front. Due to the longer ignition delays of

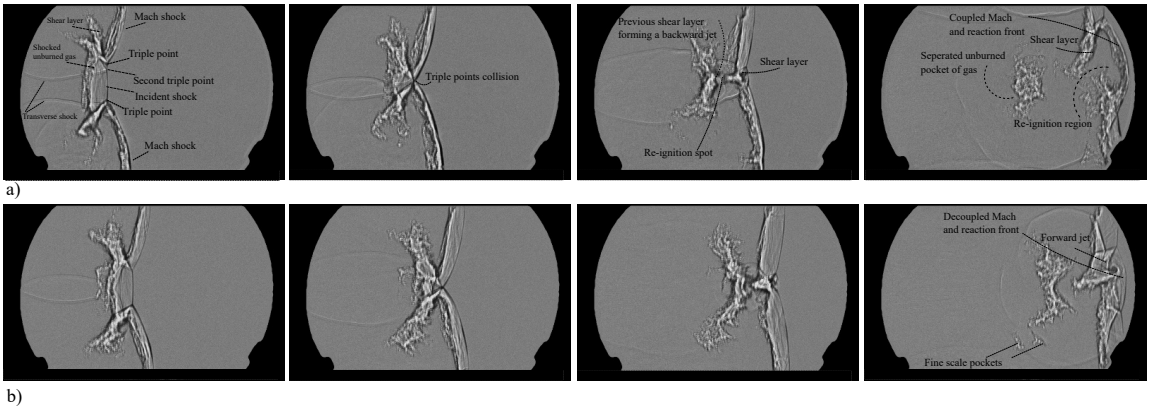

Figure 4: Detonation propagation from left to right in a $CH_4/2O_2$ mixture at $p_0 = 17.2$ kPa and $T_0 = 295$ K. The visualization length is 300 mm, captured using the schlirien technique, with a channel height H of 203 mm.

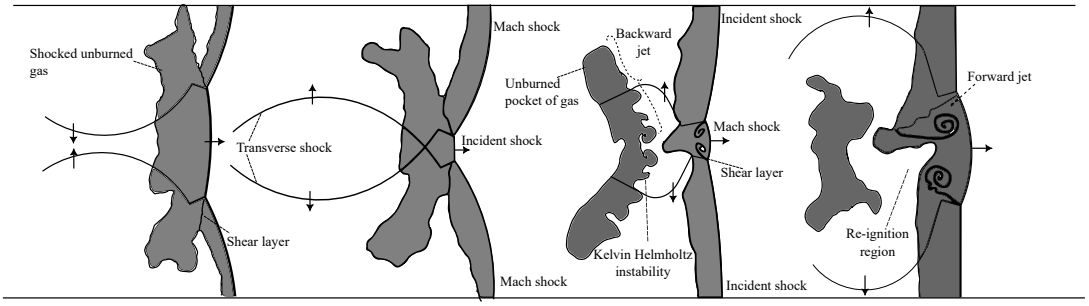

Figure 5: Illustration of the formation of the unburned pocket islands.

shocked gases processed by the weaker incident shock, the reaction zones appear thicker compared to those behind the stronger Mach shock. The tongue-like region of unreacted gases accumulates along the shear layers until a triple-point collision occurs, leading to the formation of dense, unburned gas pockets that detach from the main front. Kelvin-Helmholtz instabilities develop along both detached shear layers and the newly formed shear layer behind the Mach shock. The passage of the transverse wave through the shear layers induces further Richtmyer–Meshkov instability [4]. Additionally, the transverse wave heats the gas, which may lead to auto-ignition. After the formation of the Mach shock, the contact surface curls into a forward jet near the Mach stem. The role of this forward jet is discussed in detail in the work of Lau-Chapdelaine et al. [9]. Figure 4 compares two different outcomes of this phenomenon. In Fig. 4a, the Mach shock formed from wall reflections is stronger than in Fig. 4, which is evident from the amount of unburned gas accumulated behind the shocks. In Fig. 4, the forward jet behind the Mach shock, generated after the reflection, efficiently mixes the gas, forming hot spots that ignite the mixture, leading to the formation of coupled Mach shocks and reaction fronts. Conversely, in Fig. 4, although the presence of the jet is visible, it does not trigger ignition. For clarity, annotations have been added to the experimental images, and additional labels in Fig. 5 may help the reader with terminology. Furthermore, Fig. 6 shows the speed evolution of the shock front extrated from the centerline of the shocktube. Figure 6a shows the non-dimensional detonation velocity, normalized by the CJ velocity, as a function of distance, where zero corresponds to the exit of the diverging section. The detonation velocity remains slightly above the CJ value up to the throat and then decelerates rapidly in the diverging section. The multiple curves in the figure represent five repeated experiments. Figure 6b indicates that beyond the diverging section, the detonation velocity remains relatively constant at approximately $0.55\,D_{\mathrm{CJ}}$.

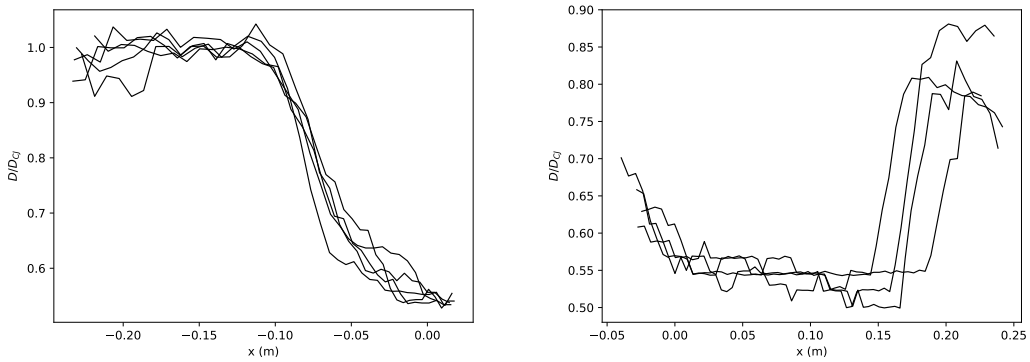

(a) Shock speed in the C-D section.

(b) Shock speed in the channel after the C-D section.

Figure 6: Non-dimensional shock velocity extracted along the centerline of the shock tube across the entire test section, based on five repeated experiments. The origin (zero) corresponds to the exit of the diverging section.

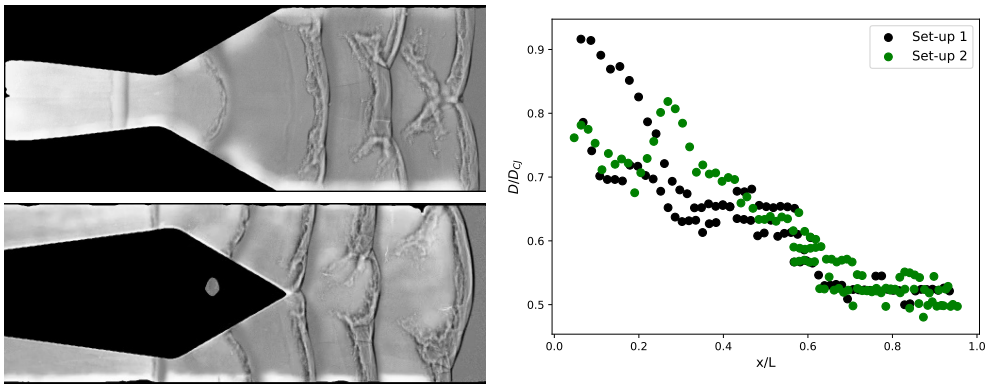

(a) Schlieren results from this work, Setup 1 (top) and previous work [7], Setup 2 (bottom).

(b) Non-dimensional velocity versus distance.

Figure 7: Comparison between the experimental set up used in this study and our previous work [7].

However, following the reflection of the two triple points along the centerline, there is a sudden increase in velocity, reaching approximately $0.85\, D_{\mathrm{CJ}}$.

3 State of the Unburned Pocket

The pressure evolution of unburned pockets can be inferred from transducer signals recorded after the shock passage. In the current setup, the reflection occurs along the centerline (Fig. 7a, top), whereas in a previous study [7] it occurred along the top wall (Fig. 7a, bottom), where the pressure sensors are mounted. The similar reflection geometry allows for qualitative comparison between the two setups. Figure 7b shows the non-dimensional velocity profiles along the top, bottom, and centerline from just after the exit of the diverging section to the triple-point reflection. The distance is scaled by L, defined as the distance between the first and second reflections. The velocity profiles exhibit similar trends across the two setups, suggesting comparable flow behavior and pocket dynamics.

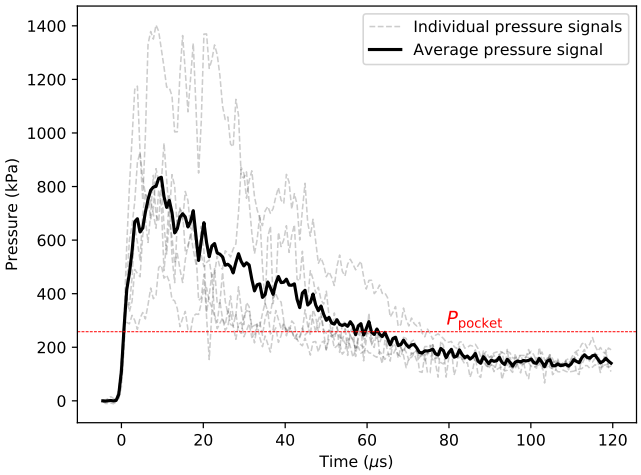

Figure 8: Temporal evolution of the incoming wave pressure measured on the top wall.

Using repeated experiments under the same conditions, we extracted the pressure signal over time from the sensor located on the top wall, where the reflection occurs. Figure 8 shows the individual pressure signals from each experiment as gray dashed lines, with the solid black line representing their average. Time zero corresponds to the shock arrival, at which point the pressure rises to approximately 800 kPa on average. The pressure then decays, potentially reaching as low as 200 kPa. However, by the time the unburned pocket forms (around 60 µs) and the transverse wave fully passes through it, the pressure stabilizes at approximately 250 kPa $\pm$ 20 kPa. While pressure is a key parameter, determining the flame speed also requires knowledge of the pocket's temperature. We assume that the gas in the pocket undergoes an isentropic process after passing through the shock, which allows us to estimate the pocket temperature using the relation $T_{\text{pocket}} = p_{\text{pocket}} \left(\frac{p_s}{T_s}\right)^{\frac{\gamma-1}{\gamma}}$, where p_{pocket} is the pressure in the pocket, and p_s and T_s are the pressure and temperature after the gas was shocked for the first time. This assumption is justified because, although transverse waves propagate through the gas after its formation, their amplitude is small (with Mach number $M \approx 1.1$), implying limited entropy generation.

To apply the isentropic relation, it is necessary to determine the thermodynamic state of the gas immediately after shock passage. Using the measured shock trajectory along the centerline—from the early times in the converging section up to the moment of triple-point reflection—and assuming a negligible post-shock velocity gradient ($du/dx = 0$), the shock jump conditions can be used to estimate the post-shock velocity. By tracking a fluid particle in the shocked, unburned gas and integrating its motion backward in time, we can determine the location where it originally crossed the shock front. Repeating this process for multiple experiments reveals that the gas most likely crosses the shock in the diverging section, as shown in Fig. 9. Accounting for velocity non-uniformities may shift this crossing point slightly downstream, closer to the end of the diverging section; however, the shock velocity remains nearly constant in that region, as shown in Fig. 6b.

Knowing the strength of the pocket at that state, we can estimate the post-shock properties, the pressure (p_s) and temperature (T_s). To account for the full range of possible thermodynamic states of the pocket, we consider a pressure range from 200 to 800 kPa. Using the isentropic relation, the corresponding temperature is calculated, typically around 800 K but potentially reaching up to 1000 K depending on the pressure. The results are shown in Fig. 10a.

Based on the thermodynamic state of the pocket, the ignition delay time is computed using constant-

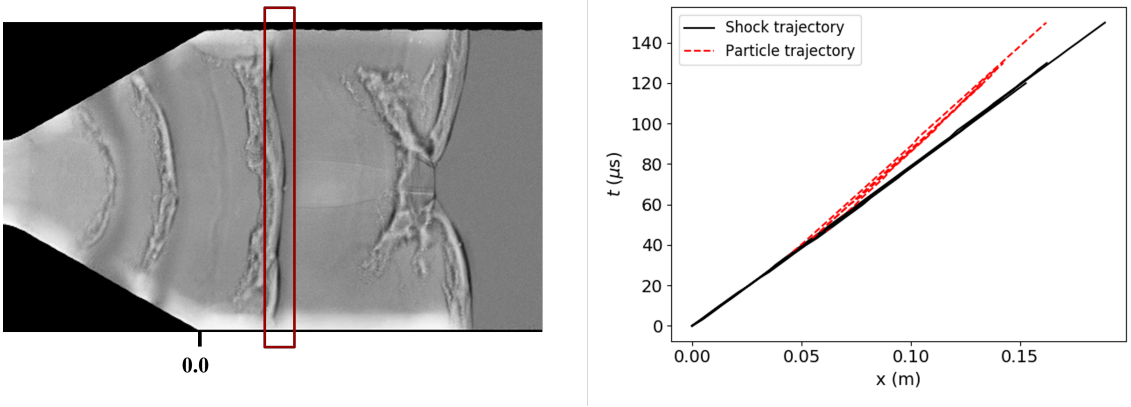

Figure 9: Left: Shadowgraph image of shock propagation in the channel. Right: Reconstructed shock and particle trajectories from the experiment.

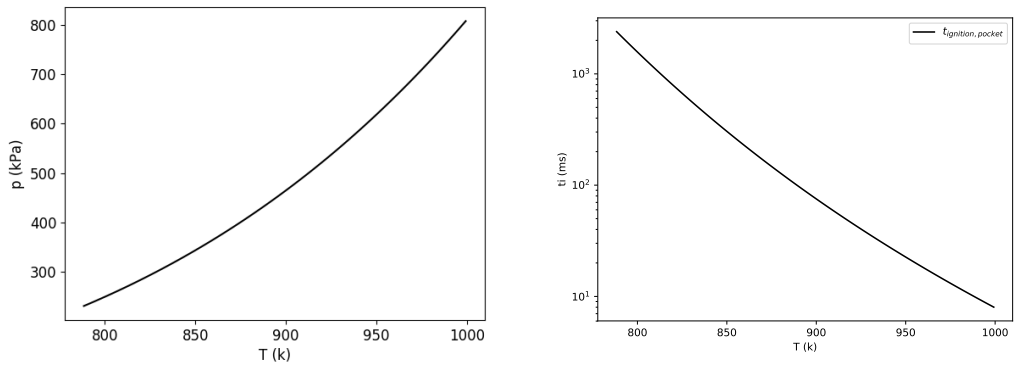

(a) Pressure and temperature of the pocket.

(b) Ignition delay time of the pocket.

Figure 10: (a) Pocket pressure measured by the pressure transducer and temperature estimated using the isentropic relation. (b) Ignition delay time of the pocket as a function of temperature.

volume combustion calculations, as shown in Fig. 10b. The results indicate that $t_{\text{ignition}} = 40\text{–}10000 \times t_{\text{pocket}}$, suggesting that ignition is most likely occurring through a diffusion-driven process. Furthermore, using the determined state of the pocket, a `FreeFlame` simulation in `Cantera` was performed to calculate the laminar flame speed, which was found to be 12 ± 2 m/s.

4.1 Experimental Determination of Pocket Burning Velocity

As shown in Fig. 4, the tongue-shaped unburned gas pockets along the turbulent shear layers display wrinkled surfaces and rough boundaries, indicative of strong hydrodynamic instabilities. Estimating the burning velocity of such pockets is challenging due to the difficulty in accurately defining their shape and surface area. Following the approach of Maxwell et al. [4], the pocket's volume and perimeter after detachment from the front are manually traced to estimate a characteristic length scale. This method, though subjective, yields a burning velocity of approximately 40 m/s. Alternatively, tracking the inward propagation speed of the flame front across three regions—upper, center, and lower—gives a higher estimate of around 100 m/s. The first method assumes a two-dimensional structure, which may not be accurate given that the pocket features are smaller than the channel thickness. The second approach

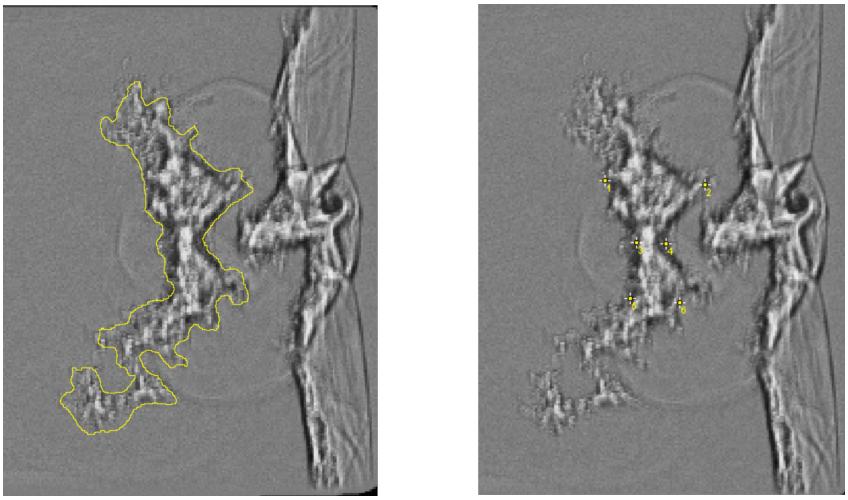

Figure 11: Left: Method 1, manual tracing of the pocket to estimate a characteristic length scale. Right: Method 2, measurement of the inward advancement of the flame front.

reflects how the flame front advances into the pocket and results in a value about seven times the laminar flame speed. Figure 11 provides an illustration of both methods. Overall, flow instabilities behind the leading shock enhance turbulent mixing and significantly affect the burning rate of the unburned pockets.

5 Conclusion

By reproducibly generating Mach reflections, we isolate the formation of unreacted gas pockets—an essential feature of cellular structures in detonations with irregular dynamics. The thermodynamic state of the pockets is measured experimentally, and analysis across repeated experiments indicates that diffusion, rather than autoignition, is the dominant burning mechanism. This new experimental setup effectively captures the key features of the detonation cellular cycle and provides a valuable approach for investigating the coupling between energy release from pockets and the motion of the lead shock.

Acknowledgments

M. I. Radulescu acknowledges the financial support provided by AFOSR grant FA9550-23-1-0214, with Dr. Chiping Li as program monitor and the Natural Sciences and Engineering Research Council of Canada (NSERC) through the Discovery Grant ”Predictability of detonation wave dynamics in gases: experiment and model development”.

References

[1] J. Lee, The detonation phenomenon, Cambridge University Press, 2008.

[2] V. A. Subbotin, Collision of transverse detonation waves in gases, Combustion, Explosion and Shock Waves 11 (1975) 411–414.

[3] E. Oran, T. Young, J. Boris, J. Picone, D. Edwards, A study of detonation structure, the formation ofunreacted gas pockets, in: Symposium International on Combustion, Vol. 19, Elsevier, 1982, pp. 573–582.

[4] B. M. Maxwell, R. R. Bhattacharjee, S. S. Lau-Chapdelaine, S. A. Falle, G. J. Sharpe, M. I. Radulescu, Influence of turbulent fluctuations on detonation propagation, Journal of Fluid Mechanics 818 (2017) 646–696.

[5] M. Radulescu, G. Sharpe, J. Lee, C. Kiyanda, A. Higgins, R. Hanson, The ignition mechanism in irregular structure gaseous detonations, Proceedings of the Combustion Institute 30 (2) (2005) 1859–1867.

[6] F. Zangene, Study of the cellular detonation dynamics at the sub-cell and macro scales, Ph.D. thesis, University of Ottawa (2025).

[7] F. Zangene, M. Radulescu, The critical conditions for the re-ignition and detonation formation from mach reflections of curved decaying shocks, Proceedings of the Combustion Institute 40 (1-4) (2024) 105774.

[8] R. Bhattacharjee, Experimental investigation of detonation reinitiation mechanisms following a mach reflection of a quenched detonation, Master's thesis, University of ottawa (2013).

[9] S. Lau-Chapdelaine, Q. Xiao, M. Radulescu, Viscous jetting and mach stem bifurcation in shock reflections: experiments and simulations, Journal of Fluid Mechanics 908 (2021) A18.